Density Gradient Stabilization of Electron Temperature Gradient Driven Turbulence in a Spherical Tokamak

Y. Ren,[1] S. M. Kaye,[1] E. Mazzucato,[1] W. Guttenfelder,[1] R. E. Bell,[1] C. W. Domier,[2] B. P. LeBlanc,[1] K. C. Lee,[2] N. C. Luhmann, Jr.,[2] D. R. Smith,[3] and H. Yuh[4]

[1]*Princeton Plasma Physics Laboratory, Princeton, New Jersey 08543, USA*
[2]*University of California at Davis, Davis, California 95616, USA*
[3]*University of Wisconsin-Madison, Madison, Wisconsin 53706, USA*
[4]*Nova Photonics, Inc., Princeton, New Jersey 08540, USA*
(Received 19 December 2010; published 22 April 2011)

In this Letter we report the first clear experimental observation of density gradient stabilization of electron temperature gradient driven turbulence in a fusion plasma. It is observed that longer wavelength modes, $k_\perp \rho_s \lesssim 10$, are most stabilized by density gradient, and the stabilization is accompanied by about a factor of 2 decrease in the plasma effective thermal diffusivity.

Microinstabilities in fusion plasmas, e.g., ion temperature gradient (ITG) mode, trapped electron mode (TEM), and electron temperature gradient (ETG) mode, could drive microturbulence, a major candidate in producing anomalous transport. Understanding, and thus controlling, microinstabilities is one of the most challenging problems in the controlled magnetic fusion research. In the literature, the density gradient has been predicted to be able to stabilize ITG and ETG, but to stabilize or destabilize TEM depending on collisionality [1]. The stability of these microinstabilities can be quantified by the critical temperature gradient at which an instability is marginally unstable. For example, an analytic form of the critical temperature gradient for ETG instability is derived as in Ref. [2]:

$$(R_0/L_{T_e})_{\text{crit}} = \max\left\{\left(1 + Z_{\text{eff}}\frac{T_e}{T_i}\right)(1.33 + 1.99\hat{s}/q) \right.$$
$$\left. \times (\ldots), 0.8R_0/L_{n_e}\right\}, \quad (1)$$

where R_0 is the major radius of the flux surface center, $L_{T_e} = (d\ln T_e/dr)^{-1}$ is the electron temperature scale length, $L_{n_e} = (d\ln n_e/dr)^{-1}$ is the electron density scale length, Z_{eff} is the effective ionic charge, T_e is the electron temperature, T_i is the ion temperature, $\hat{s} = (r/q)(dq/dr)$ is the magnetic shear, q is the magnetic safety factor, and $(\ldots)$ denotes some geometric terms not easily quantifiable for low aspect ratio tokamaks. It can be seen from this formula that, if large enough, the density gradient term, $0.8R_0/L_{n_e}$, could determine the critical temperature gradient alone and result in the stabilization of ETG modes. Confinement improvements have been observed to be associated with peaked density profile resulting from pellet injection [3], and the improvements were attributed to density gradient, perpendicular flow shearing, and/or reversed magnetic shear [4–6]. Here we present the first direct experimental demonstration of density gradient

stabilization of electron-gyro scale turbulence. The experimental observation is in quantitative agreement with linear numerical simulations and supports the conclusion that the observed density fluctuations are driven by ETG. Furthermore, it is found that the longer wavelength modes, $k_\perp \rho_s \lesssim 10$ (ρ_s is the ion gyroradius at electron temperature and $k_\perp$ is the wave number perpendicular to local equilibrium magnetic field), are strongly stabilized by density gradient and that plasma effective thermal diffusivity is decreased by about a factor of 2 along with the stabilization.

The measurement was carried out on the National Spherical Torus Experiment (NSTX) with a 280 GHz collective microwave scattering system (the high-k scattering system) [7]. This scattering system has five channels covering a wave number range of $5 \lesssim k_\perp \lesssim 30 \text{ cm}^{-1}$ with a wave number resolution about 1 cm^{-1} and a radial resolution of $\triangle R \approx \pm 2$ cm, which allows us to study the evolution of local fluctuation with respect to local equilibrium quantities, e.g., L_{T_e}, L_{n_e}, q, and $\hat{s}$.

Figure 1 shows the density (a) and temperature (b) profiles at $t = 498$ ms [before an event of edge localized mode (ELM) [8]] and at $t = 532$ ms (after the ELM event) measured by multiple point Thompson scattering (MPTS) [9] of shot 140 620, a deuterium H-mode plasma with 900 kA plasma current and 4.5 kG toroidal field. The measurement region of the high-k scattering system, the overall radial region covered by all channels with the center of scattering location separated by $\lesssim 1$ cm, is from about $R = 134$ to 139 cm. A large increase in density gradient after the ELM event in the measurement region is evident in Fig. 1(a), and only a small change in electron temperature profile is seen in Fig. 1(b). We also note that magnetic measurements show no large amplitude global MHD activity before, during, and right after the ELM event.
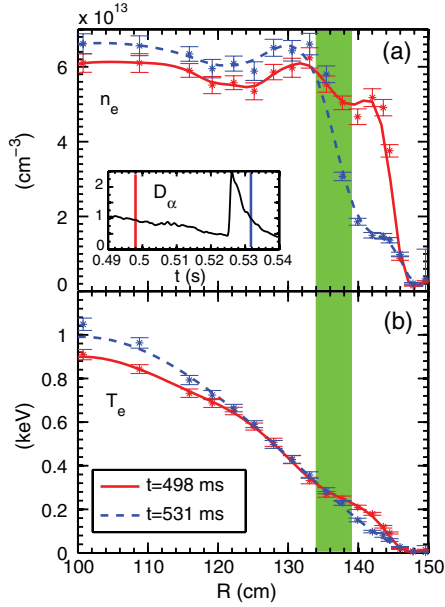
FIG. 1 (color online). (a) Radial profiles of electron density at $t = 498$ and 532 ms which are before and after an ELM event (see the inserted D_α signal, where the two vertical lines denote the two Thompson time points). (b) Radial profiles of electron temperature at $t = 498$ and 532 ms. The shaded regions denote the measuring region of the high-k system. Large change in L_{n_e} after the ELM at $t = 532$ ms is evident.

Figure 2 shows the spectrograms of channels 2 and 3 of the high-k system and the frequency spectra at three MPTS time points, $t = 498, 515$ (before the ELM event) and 532 ms (after the ELM event). The wave numbers measured by the two channels are $k_\perp \rho_s \approx 10$–12 (channel 2)

and 8–10 (channel 3) before the ELM event, and become 15–17 and 12.5–14.5 after the ELM event due to a larger refraction following the ELM event. The signal from the collective scattering of microwave by electron density fluctuations manifests as spectral peaks at negative frequencies, corresponding to the ion diamagnetic direction in the laboratory frame. However, accounting for a Doppler shift of $k_T V_T / 2\pi$ (the vertical green lines in the lower panels denote $k_T V_T / 2\pi$ at $t = 498$ ms), where k_T is the toroidal wave number and V_T is the plasma toroidal flow, the wave propagation direction in the plasma frame is in the electron diamagnetic direction, consistent with previous results [10]. The large central peaks at $f = 0$ are due to the spurious reflection of the probing microwave beam, and large frequency separations between the scattering signals and the central peaks ensure accurate measurements of scattered microwave power. It can be immediately seen from the figure that the two channels show large reduction in scattering signal power after the ELM event, and most notably, the scattering signals received by channel 3 are below its noise level. However, since the wave numbers measured by the high-k channels increase after the ELM event, the change of wave number spectrum has to be assessed as below.

Figure 3 shows the normalized $k_\perp$ spectra in arbitrary units at the three MPTS time points. At $t = 532$ ms, estimated upper bounds are plotted for channels 3 and 4, since they have scattering signals below the noise level. The upper bounds of possible fluctuation power are estimated by using the scattering signal power of channel 5 at $t = 532$ ms, which is about 3 times higher than noise level, to obtain a minimum detectable scattering power (channel 5
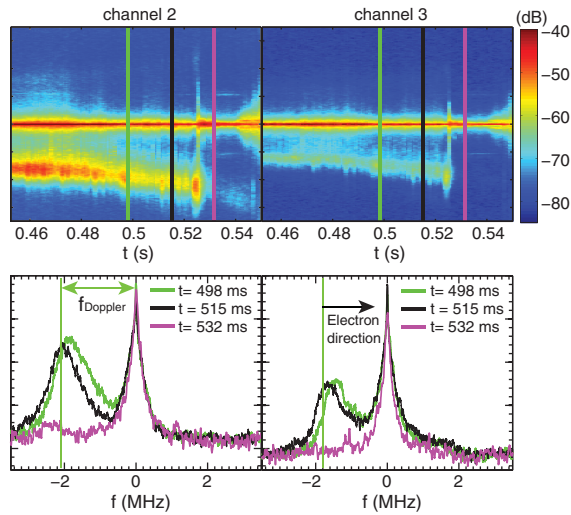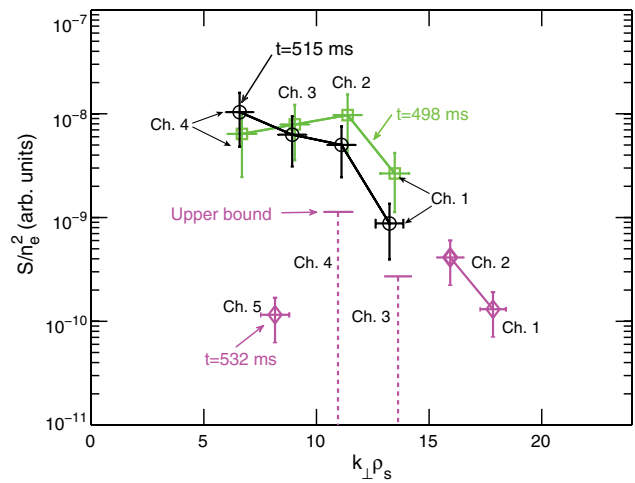

FIG. 2 (color). Upper panels: The spectrograms of two high-k channels around the ELM event. Lower panels: The frequency spectra at the three exact MPTS time points, $t = 498, 515$, and 532 ms, for the two high-k channels. The three colored lines in the upper panels denote time points used for plotting the lower panels with the same color coding.

FIG. 3 (color online). The $k_\perp$ spectra in arbitrary unit (normalized to n_e^2 and S is the spectral density calculated using the total scattered power in the spectra of each channel) at the three MPTS time points. Data points are also labeled with their corresponding channel numbers. The absolute upper bounds for the density fluctuation spectral power are denoted by horizontal solid lines on the tops of vertical dashed lines.

has similar noise level as channels 3 and 4). It is clear from Fig. 3 that after the ELM event, i.e., at $t = 532$ ms, the fluctuation power for $k_\perp \rho_s \lesssim 15$ is reduced and the most significant reduction, more than an order of magnitude, occurs at small wave numbers, $k_\perp \rho_s \lesssim 10$. We note that the actual reduction in spectral power in channels 3 and 4 could be more than denoted by the upper bounds. Interestingly, the fluctuation power at higher wave numbers, $k_\perp \rho_s \gtrsim 15$, seems to be unaffected by the increase of density gradient; i.e., an overlap in fluctuation power is expected if one extrapolates the $k_\perp$ spectrum at $t = 515$ ms with a power law to higher wave numbers. We also note that channel 5 is not included in the two $k_\perp$ spectra before the ELM event since its scattering location is separated for more than 2 cm from those of the other four channels for those particular density profiles. However, this channel is included in the $k_\perp$ spectrum at $t = 532$ ms since the change of density profile after the ELM event leads to a better overlap of the radial scattering locations of different channels with separations of the center of scattering location $\lesssim 1$ cm.

In order to demonstrate the fact that the density gradient has the largest change (increase) in the high-k measurement region after the ELM event, the time evolutions of four equilibrium quantities around the ELM event are plotted at the three MPTS time points in Fig. 4. The error bars in the figure represent profile variations in high-k measurement regions for channels measuring the wave numbers experiencing the largest change in spectral power after the ELM event, namely, channels 3 and 4 before the ELM event (from about $R = 134.5$ to 138.5 cm) and channels 4 and 5 after the ELM event (from about $R = 134$ to 138 cm). The normalized electron density gradient, R_0/L_{n_e}, and normalized electron temperature gradient, R_0/L_{T_e}, are obtained from the MPTS profiles. T_i and normalized ion temperature gradient R_0/L_{T_i} are obtained from charge exchange recombination spectroscopy measurement [11]. It is easy to see from Fig. 4 that the greatest change in the equilibrium quantities after the ELM
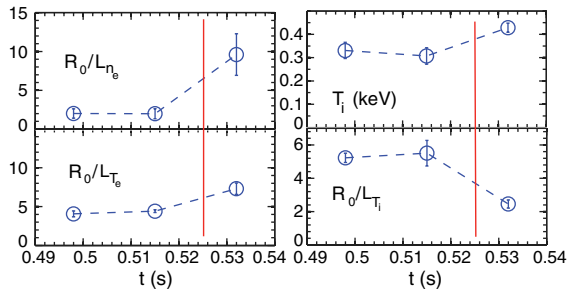

FIG. 4 (color online).   The normalized electron density gradient, R_0/L_{n_e}, normalized electron temperature gradient, R_0/L_{T_e}, ion temperature, T_i, and normalized ion temperature gradient, R_0/L_{T_i}, at $t = 498$, 515, and 532 ms averaged in the high-k measurement locations (see main text). The timing of the ELM event is denoted by the red vertical solid lines.

event is the factor of 5 increase of R_0/L_{n_e}. The next largest changes are the 60% increase in R_0/L_{T_e} and the 60% decrease in R_0/L_{T_i}. Despite the increase in the T_e gradient which drives ETG modes, the turbulence spectral power has been shown to be significantly decreased as shown in Fig. 3. The decrease in R_0/L_{T_i} should only affect the stability of ITG modes. However, the observation of neoclassical ion transport level in NSTX H-mode plasmas indicates that ITG modes are stabilized by geometrical and $E \times B$ shear effects [12]. In addition to changes in gradients, a 40% increase in T_i decreases T_e/T_i (T_e change is smaller), a destabilizing effect as shown in Eq. (1). However, we will show later that the density gradient change is so large that, as described in Eq. (1), the second term in the "max" function overcomes the first term. Finally, we note that all other relevant equilibrium quantities, T_e, n_e, $\hat{s}$, q, Z_{eff}, and the Hahm-Burrell $E \times B$ shear rate [13], show less than 25% change after the ELM event.

The observed density gradient stabilization is in good agreement with stability analysis performed with the GS2 code [14]. GS2 is an initial value gyrokinetic code which, in its linear mode, finds the fastest growing mode for a given pair of poloidal and radial wave numbers. In order to find the critical temperature gradient, growth rates of a range of unstable poloidal wave numbers are calculated with several different temperature gradients. Linear extrapolation of the growth rate of the most unstable mode determines the critical temperature gradient [2]. In Fig. 5, the critical T_e gradients in the high-k measurement region were calculated using GS2 and are plotted for the three MPTS time points, i.e., Figs. 5(a)–5(c), together with the measured T_e gradient profile. It can be seen from Fig. 5 that at the time points before the ELM event, i.e., 498 ms (a) and 515 ms (b), the measured T_e gradients are larger than the critical T_e gradients from GS2 calculation in most of the high-k measurement region. However, at $t = 532$ ms (c), after the ELM event, the critical T_e gradient from GS2 calculations is much larger than the measured T_e gradient for most of the high-k measurement region; i.e., ETG modes are linearly stable, which is able to explain the observed large reduction of spectral power for $k_\perp \rho_s < 10$ at $t = 532$ ms as shown in Fig. 3. We note that, due to the small size of the existing ETG unstable region, where $(R_0/L_{T_e})_{\text{measured}} > (R_0/L_{T_e})_{\text{critic,GS2}}$, in Fig. 5(c), it may not be enough to explain the unaffected spectral power for $k_\perp \rho_s \gtrsim 15$ in Fig. 3. In order to show that the density gradient increase is responsible for the large increase of critical T_e gradient in Fig. 5(c), critical T_e gradients calculated with R_0/L_{n_e} decreased by 3, 4.5, and 6 units are also plotted in Fig. 5(c). It is clear that $(R_0/L_{n_e} - 3)$ leads to significantly lowered critical T_e gradients in the high-k measurement region. However, while the decreases to $(R_0/L_{n_e} - 4.5)$ and $(R_0/L_{n_e} - 6)$ lead to further reduction of critical R_0/L_{T_e} at $R > 135.5$ cm, only a small change in critical R_0/L_{T_e} is observed at $R \lesssim 135$ cm, which is
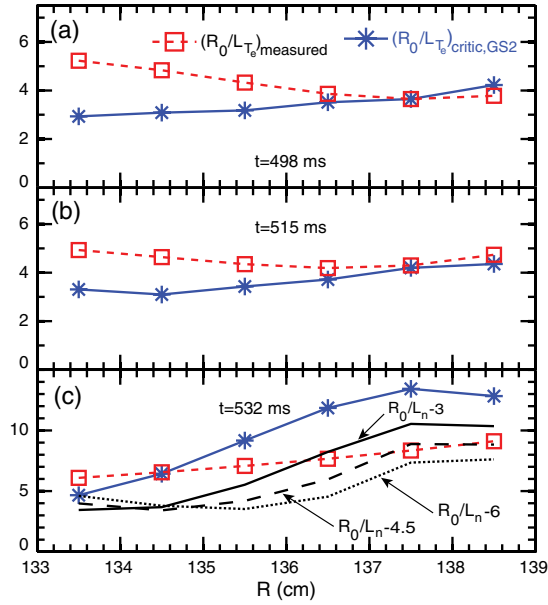
FIG. 5 (color online). The critical T_e gradients calculated by
GS2, $(R_0/L_{T_e})_{\text{critic,GS2}}$, (asterisks) in comparison with the measured
temperature gradient, $(R_0/L_{T_e})_{\text{measured}}$, (open squares) in the
high-k measurement region: (a) at $t = 498$ ms, (b) $t = 515$ ms,
(c) $t = 532$ ms. Additional lines in (c) denote $(R_0/L_{T_e})_{\text{critic,GS2}}$
calculated with $(R_0/L_{n_e} - 3)$ (solid line), $(R_0/L_{n_e} - 4.5)$ (dashed
line), and $(R_0/L_{n_e} - 6)$ (dotted line).

consistent with the fact that the first term in the max
function of Eq. (1) dominates the critical R_0/L_{T_e} as
the second density gradient term becomes sufficiently
small.

The stabilization of the electron-scale turbulence is also
found to be accompanied by an improvement in plasma
confinement. The transport analysis was carried out
with TRANSP [15]. Because of a strong energy coupling
between electrons and ions due to large plasma density
($n_e \sim 5 \times 10^{19}$ m^{-3}), here we show the plasma effective
thermal diffusivity, χ, in Fig. 6 as a function of R at the
three MPTS time points: $t = 498$, 515, and 532 ms, where
a factor of about 2 reduction in χ can be seen in the high-k
measurement regions used in Fig. 4 at $t = 532$ ms after the
ELM event. (We note that the uncertainty in χ in the
shaded region in Fig. 6 is about 30%.) This correlation
suggests that the reduction in the longer wavelength
modes, $k_\perp \rho_s < 10$, may be responsible for the improve-
ment in plasma confinement.

In conclusion, we have demonstrated the density gra-
dient stabilization of electron-scale turbulence by showing
significant reduction in density fluctuation spectral power
at $k_\perp \rho_s \lesssim 10$ following a large density gradient increase
induced by an ELM event. This observation together with
linear gyrokinetic stability analysis supports the fact that
the turbulence we observe before the ELM event is driven
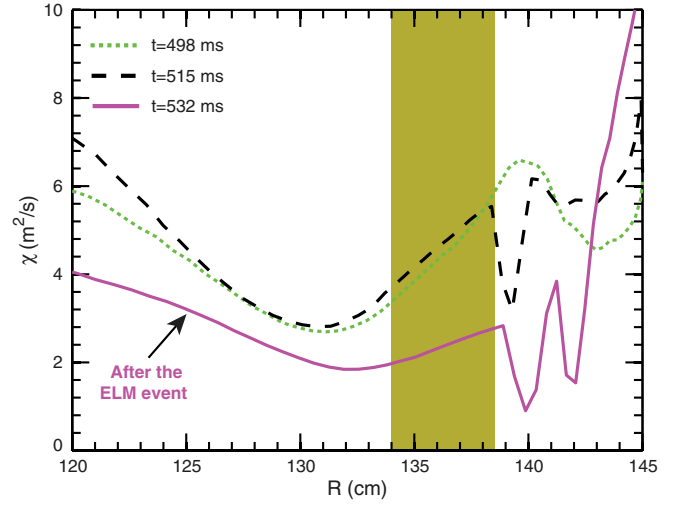by ETG instability. TEM, on the other hand, is ruled out by

FIG. 6 (color online). The plasma effective thermal diffusivity
as a function of R for the three MPTS time points: $t = 498$
(dotted line), 515 (dashed line), and 532 ms (solid line) with the
shaded region denoting the high-k measurement regions as used
in Fig. 4 (from about $R = 134$ to 138.5 cm).

this observation, since our ion-scale GS2 calculations (not
shown) show that TEM should be destabilized by the large
density gradient. A reduction in plasma effective thermal
diffusivity is also found to be correlated with the significant
reduction of spectral power at $k_\perp \rho_s \lesssim 10$, suggesting the
importance of these modes in driving anomalous plasma
thermal diffusion.

[1] M. Romanelli *et al.*, Phys. Plasmas **11**, 3845 (2004).
[2] F. Jenko *et al.*, Phys. Plasmas **8**, 4096 (2001).
[3] M. Greenwald *et al.*, Phys. Rev. Lett. **53**, 352 (1984).
[4] B. Balet *et al.*, Nucl. Fusion **30**, 2029 (1990).
[5] P. Maget *et al.*, Nucl. Fusion **39**, 949 (1999).
[6] F. Romanelli and S. Briguglio, Phys. Fluids B **2**, 754
     (1990).
[7] D. R. Smith *et al.*, Rev. Sci. Instrum. **79**, 123501 (2008).
[8] H. Zohm, Plasma Phys. Controlled Fusion **38**, 105 (1996).
[9] B. P. LeBlanc *et al.*, Rev. Sci. Instrum. **74**, 1659 (2003).
[10] E. Mazzucato *et al.*, Phys. Rev. Lett. **101**, 075001 (2008).
[11] R. E. Bell, Rev. Sci. Instrum. **77**, 10E902 (2006).
[12] S. M. Kaye *et al.*, Phys. Rev. Lett. **98**, 175002 (2007).
[13] T. S. Hahm and K. H. Burrell, Phys. Plasmas **2**, 1648
     (1995).
[14] M. Kotschenreuther *et al.*, Comput. Phys. Commun. **88**,
     128 (1995).
[15] R. J. Hawryluk, *Physics of Plasma Close to
     Thermonuclear Conditions* (Pergamon, New York, 1981).